ACS Medicinal Chemistry Letters

Open Access

pubs.acs.org/acsmedchemlett

Letter

Molecular Striptease of a Thiadiazolopyrimidine Hit Yields a Streamlined, Artifact-Free NADPH Mimic for NOX Inhibition

Emanuele Fabbrizi,[¶] Andrea Mancini,[¶] Chiara Lambona, Salvatore Macrì, Marianna Nalli, Francesco Quilli, Federico Pandolfi, Domenico Raimondo, Sara Marchese, Andrea Mattevi, Jihyeon Lee, Minhye Choi, Yun Soo Bae, Nadya Hristova-Avakumova, Magdalena Kondeva-Burdina, Denitsa Stefanova, Neda Anastassova, Sergio Valente, Dante Rotili, and Antonello Mai*

Cite This: https://doi.org/10.1021/acsmedchemlett.6c00370

Read Online

ACCESS | Metrics & More | Article Recommendations | Supporting Information

ABSTRACT: The convergence of oxidative stress and inflammation drives neurodegeneration and cancer, positioning NADPH oxidases (NOXs) as critical therapeutic targets. Starting from the polyfunctional thiadiazolopyrimidine hit **1**, we systematically truncated its peripheral arms to map minimum pharmacophoric requirements. While extensive clipping compromised activity, strategic optimization yielded the streamlined analogue **5**. In silico, **5** acted as a competitive NADPH mimic; in cell-free assays, it maintained multi-isoform potency, inhibiting NOX1 and NOX5 at low-micromolar concentrations. In rat brain subcellular fractions, **1** and **5** demonstrated concentration-dependent neuroprotective and antioxidant efficacy (1−10 μM) by suppressing lipid peroxidation and preserving mitochondrial and synaptosomal viability. Notably, chemical profiling proved that **5** successfully stripped away the pro-oxidant liabilities and radical-scavenging artifacts inherent to **1**. In cancer, **1** displayed some antiproliferative activity, mainly in hematological malignancies. Compound **5**, although aqueous solubility issues limited its cellular antiproliferative performance, represents a specific, artifact-free architectural starting point for future selective NOX inhibitor development.

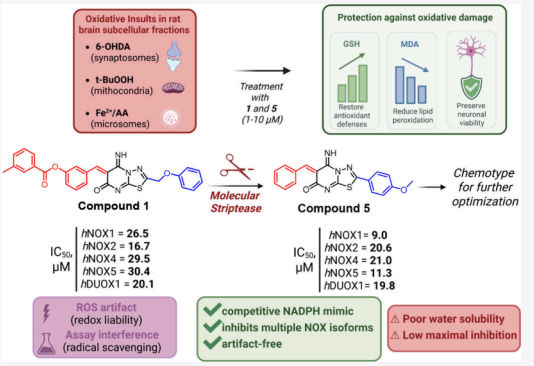

KEYWORDS: *NOX inhibitors, Thiadiazolopyrimidine, Scaffold truncation, Neuroprotection, Redox liabilities*

Neurodegenerative disorders and cancer are increasingly recognized as multifactorial pathologies driven by the convergence of oxidative stress and chronic inflammation.[1−4] Among the enzymatic sources of pathological reactive oxygen species (ROS), NADPH oxidases (NOXs) play a prominent role.[5] While dysregulated NOX1, NOX2, and NOX4 isoforms are strongly implicated in microglial activation, blood−brain barrier dysfunction, and tumor progression,[6−14] recent evidence also links calcium-dependent NOX5 and dual oxidase 1 (DUOX1) to neurovascular injury and oncogenic redox-signaling.[15−18] Despite strong biological validation, developing small-molecule NOX inhibitors suitable for central nervous system (CNS) applications remains challenging.

Recently, via ultralarge in silico screens of about 350 million compounds utilizing VirtualFlow33 against the *Cylindrospermum stagnale* NOX5 (*cs*NOX5) dehydrogenase domain (both FAD-complexed and apo forms),[19] we identified the synthetic hit **1** (M11, Figure 1).[20] Compound **1** exhibited (sub)-micromolar inhibition in NOX membrane preparations (IC_{50} values = 0.36−40.2 μM) without structural ROS-scavenging or assay interference.[20] However, its high structural complexity and suboptimal physicochemical profile prompt further investigation into its minimal pharmacophoric requirements to enable neurotherapeutic optimization.

To address this, we applied a "molecular striptease" strategy[21,22] to dissect the contribution of individual structural motifs of **1** to NOX inhibition. We hypothesized that retaining the core NOX-interacting pharmacophore while strategically removing nonessential, bulky elements would preserve inhibitory activity, enhance chemical tractability, and provide clearer structure−activity relationships (SAR) across different NOX family members.

Starting from the multisubstituted core of **1**, we systematically clipped its peripheral arms (Figure 1): deletion of the 2-phenoxymethyl chain from the [1,3,4]thiadiazolo[3,2-*a*]-pyrimidine nucleus yielded **2**, while cleavage of the 3-methylbenzoyl moiety from the 3-hydroxybenzylidene sub-

Received: June 30, 2026
Revised: August 1, 2026
Accepted: August 3, 2026

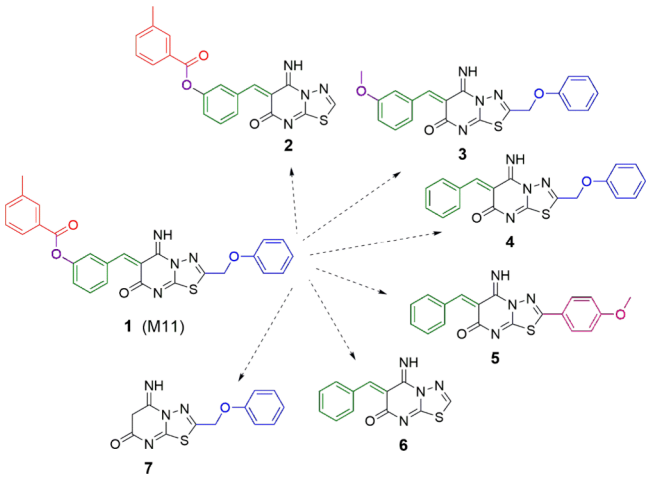

Figure 1. Chemical structures of compound **1** (M11) and simplified analogues **2**–**7**.

structure afforded **3**. Further truncation of **3** via removal of the 3-benzylidene substituent produced analogues **4** and **5**. Finally, maximizing the structural simplification of **4** by systematically deleting either the phenoxymethyl chain or the benzylidene motif yielded the minimal heterocyclic cores **6** and **7**, respectively.

CHEMISTRY

The synthesis of **1** (**M11**) and its simplified analogues **2**–**6** was accomplished starting from the key intermediates 5-imino-5,6-dihydro-7*H*-[1,3,4]thiadiazolo[3,2-*a*]pyrimidin-7-ones (**7**–**9**). These cores were prepared via cyclocondensation of the corresponding commercially available 1,3,4-thiadiazol-2-amines with ethyl cyanoacetate in anhydrous ethanol containing sodium ethoxide, followed by acidic quenching. Subsequent Knoevenagel condensation of intermediates **7**–**9** with appropriate aromatic aldehydes in a DMF/EtOH mixture under basic conditions afforded the target compounds **1**–**6** (Scheme 1). Detailed synthetic protocols and analytical characterization are provided in the Supporting Information.

BIOCHEMISTRY AND STRUCTURE–ACTIVITY RELATIONSHIPS (SAR)

Compounds **1**–**6** and intermediate **7** were evaluated against human NOX isoforms (NOX1, NOX2, NOX4, NOX5, and DUOX1) utilizing purified membrane preparations from transgenic *Drosophila* expressions. ROS production was quantified via lucigenin-amplified chemiluminescence.[23]

In this assay platform, the parental hit **1** displayed IC_{50} values of 26.5 μM (NOX1), 16.7 μM (NOX2), 29.5 μM (NOX4), 30.4 μM (NOX5), and 20.1 μM (DUOX1) (Table 2), confirming its multi-isoform activity profile with minimal 1.5- to 2.5-fold potency variation for NOX1, −2, and −4, and 84-fold lower potency for NOX5, when compared to initial screenings.[20] Analogues **2**–**7** were primary-screened at fixed 10 and 100 μM doses (Table 1); IC_{50} values were subsequently extrapolated for derivatives achieving >70% inhibition at 100 μM against at least one isoform (Table 2).

At fixed concentrations, analogue **2** (lacking the 2-phenoxymethyl chain) retained a profile comparable to **1** against NOX2 and NOX4, whereas the 3-methylbenzoyl-clipped derivative **3** showed reduced efficacy. Among the highly truncated derivatives **4** and **5**, compound **4** exhibited poor

Scheme 1. General Synthesis of M11 and its Analogues[a]

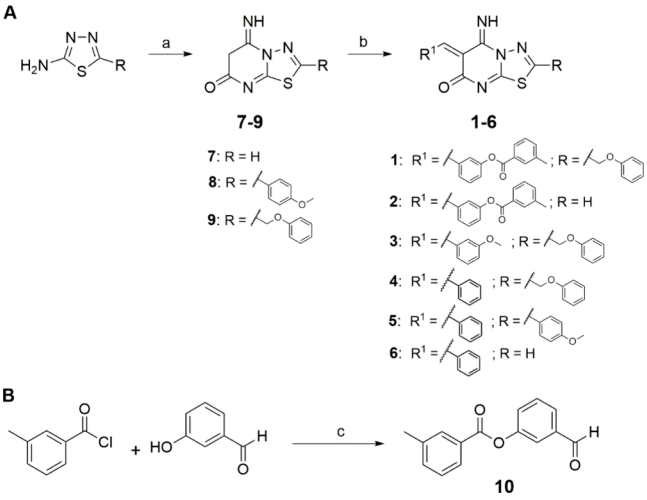

[a]Reagents and conditions: a) Na (1.0 equiv), anhydrous EtOH, ethyl cyanoacetate (1.0 equiv), reflux, 2 h; b) appropriate aromatic aldehyde (1.05 equiv), Et_3N (cat.), DMF/EtOH (1:1), 50 °C, 3 h; c) Et_3N, THF, DCM, 0 °C, 1 h.

activity. Unexpectedly, compound **5** regained prominent inhibitory potency, an effect driven by replacing the phenoxymethyl motif of **4** with a 4-methoxyphenyl group. The minimal heterocyclic cores **6** and **7** were virtually inactive.

Intriguingly, despite high screening inhibition by **2** at 100 μM, its measured IC_{50} values revealed a general drop in potency relative to **1**. Conversely, compound **5** exhibited lower or comparable efficacy to **1** at fixed high doses, bound to limited maximum inhibition (I_{max}) values. This discouraging result likely reflects the poor solubility of **5**, which hampered the compound's ability to achieve high maximal inhibition values against NOXs. Nevertheless, the apparent IC_{50} ($IC_{50,app}$) values determined for **5** revealed an inhibitory potency comparable to **1** against NOX2, NOX4, and DUOX1, alongside a 2.7- to 2.9-fold increase in potency against NOX1 ($IC_{50,app}$ = 9.0 μM) and NOX5 ($IC_{50,app}$ = 11.3 μM), breaking into the low-micromolar range. The inhibition curves for **1**, **2**, and **5** against the tested NOX isoforms are reported in Figure S1 in Supporting Information.

MOLECULAR MODELING AND BINDING DETERMINANTS OF COMPOUND 5

To elucidate the structural determinants driving the potency of the simplified analogue **5**, we cross-compared its predicted binding modes against NOX1 and NOX5 with those of **1**. Protein–ligand complexes were modeled using Boltz2, yielding high-confidence predictions (confidence scores: 0.85 for **5**-NOX5; 0.89 for **1**-NOX5).

Both compounds occupy the catalytic cofactor-binding pocket within the dehydrogenase (DH) domain of NOX5, spanning the interface of the NADPH- and FAD-binding domains (Figure 2A).[24,25] In NOX5, the binding pose of **5** overlaps extensively with the natural cofactors NADPH/$NADP^+$ from the human NOX5 cryo-EM structure (PDB: 8U87)[26] and the *cs*NOX5 crystal structure complexed with inhibitor M41 (designated as compound 3 in,[20] PDB: 8CB0) (Figure 3A). This conserved alignment suggests that the simplified architecture of **5** effectively acts as a competitive NADPH mimic.

https://doi.org/10.1021/acsmedchemlett.6c00370
ACS Med. Chem. Lett. XXXX, XXX, XXX–XXX

Table 1. Percentage of Inhibition of NOX Isoforms at Fixed Doses (10 and 100 μM) by Compounds 1−7

	% inhibition, μM									
	NOX1		NOX2		NOX4		NOX5		DUOX1	
compd	10	100	10	100	10	100	10	100	10	100
1 MC5328	30.7	81.4	41.5	81.9	29.3	82.6	26.3	71.9	31.4	80.8
2 MC5333	7	77.3	14.5	76.6	13.3	76.9	10.2	80.5	12.1	82.9
3 MC5329	20.2	46.0	15.3	51.1	26.4	52.5	14.5	54.7	31.4	56.8
4 MC5330	22.6	64.9	8.1	57.1	3.2	64.2	14.0	65.2	26.1	62.3
5 MC5335	25.6	39.3	18.7	50.8	19.7	50.3	21.9	43.7	25.1	62.9
6 MC5334	6.0	10.3	2.2	5.0	23.9	17.1	7.4	8.0	9.7	6.7
7 MC5327	10.9	4.7	−9.5	1.8	−7.4	3.3	4.4	1.9	5.5	3.4

Table 2. IC_{50} Values and Percentages of Maximum Inhibition (I_{max}) by 1, 2, and 5 against NOX1, NOX2, NOX4, NOX5, and DUOX1

compd	structure	NOX1		NOX2		NOX4		NOX5		DUOX1	
		IC_{50}[a], μM	I_{max}	IC_{50}, μM	I_{max}	IC_{50}, μM	I_{max}	IC_{50}[a], μM	I_{max}	IC_{50}, μM	I_{max}
1 MC5328	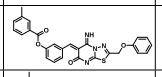	26.5	*102*	16.7	*94*	29.5	*106*	30.4	92.5	20.1	*97*
2 MC5333	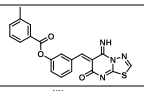	235	*>100*	80.4	*>100*	133	*>100*	161.2	*>100*	111.1	*>100*
5 MC5335	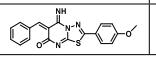	9.0	*43*	20.6	*62*	21.0	*61*	11.3	*49*	19.8	*75*

[a] $IC_{50,app}$ for compound **5**

Specifically, **5** simultaneously engages the key residues involved in NADPH recognition—R463, R595, and R671—exploiting a crucial, conserved electrostatic network within the DH domain. Additionally, its phenoxymethyl and imino-oxo-pyrimidine motifs form hydrogen bonds with S696 and F719, the latter being a highly conserved C-terminal residue critical for regulating NOX catalytic activity.[27] Hydrophobic interactions with NBD residues I593 and T631 further stabilize the complex.

Conversely, the bulkier compound **1** inserts deeper toward the FAD cofactor rather than the NADPH site (Figure 3A), partially mimicking M41's stacking triad and engaging only two of the three key arginines. This indicates a binding mode less focused on NADPH mimicry and more dependent on local structural adaptation.

High-confidence predictions were similarly obtained for NOX1 (scores: 0.89 for **5**-NOX1; 0.88 for **1**-NOX1). In these models (Figure 2B), both ligands occupy the DH domain catalytic region. Compound **5** strictly preserves the NADPH-aligned binding mode observed in NOX5, making no contact with the FAD cofactor within a 4.5 Å cutoff, and is stabilized by hydrophobic interactions with I438 and P533. Compound **1** accommodates a distinct conformation within the pocket, contacting a larger surface area due to its size, forming hydrogen bonds and π-cation interactions with R440 and R507.

In the absence of an experimentally obtained NOX1 structure, superimposition onto the human NOX2 cryo-EM structure (PDB: 8WEJ, ∼60% sequence identity)[28] confirmed that both ligands align within the solvent-exposed groove normally engaged by NADPH, without penetrating as deeply as **1** does in NOX5 (Figure 3B). To validate this competitive mechanism, a fully cofactored (FAD/NADPH) NOX1 structure was generated via Boltz2 (score: 0.9). The analysis confirmed that **5** substantially overlaps with the core NADPH architecture, while **1** aligns predominantly with its nicotinamide portion via its phenoxymethyl group.

Overall, while **1** exhibits high conformational variability across different NOX isoforms, the simplified analogue **5** maintains a highly consistent, rigid binding mode, supporting its role as a targeted competitive NADPH mimic across the NOX family.

NEUROPROTECTIVE, ANTIOXIDANT, AND RADICAL SCAVENGING PROFILES

Given the central role of NOXs in neurovascular impairment, compounds **1** and **5** were evaluated for neuroprotective efficacy against oxidative damage in human neuroblastoma SH-SY5Y cells.[29,30] Stability studies conducted on **1** in PBS at 37 °C after 4, 24, and 48 h showed no significant decrease of compound over the time course, indicating good stability for the benzoic ester of **1** under these conditions (Figure S2 in Supporting Information). MTT assays established favorable cellular tolerance, with IC_{50} values of 57.99 μM (**1**) and 53.02 μM (**5**) (Figure S3 in Supporting Information). Based on these profiles, nontoxic doses (1, 5, and 10 μM) were screened in three complementary models of neuronal injury: H_2O_2-induced oxidative stress, L-glutamate-induced excitotoxicity, and MPP^+-induced neurotoxicity. Neither compound produced a statisti-

https://doi.org/10.1021/acsmedchemlett.6c00370
ACS Med. Chem. Lett. XXXX, XXX, XXX−XXX

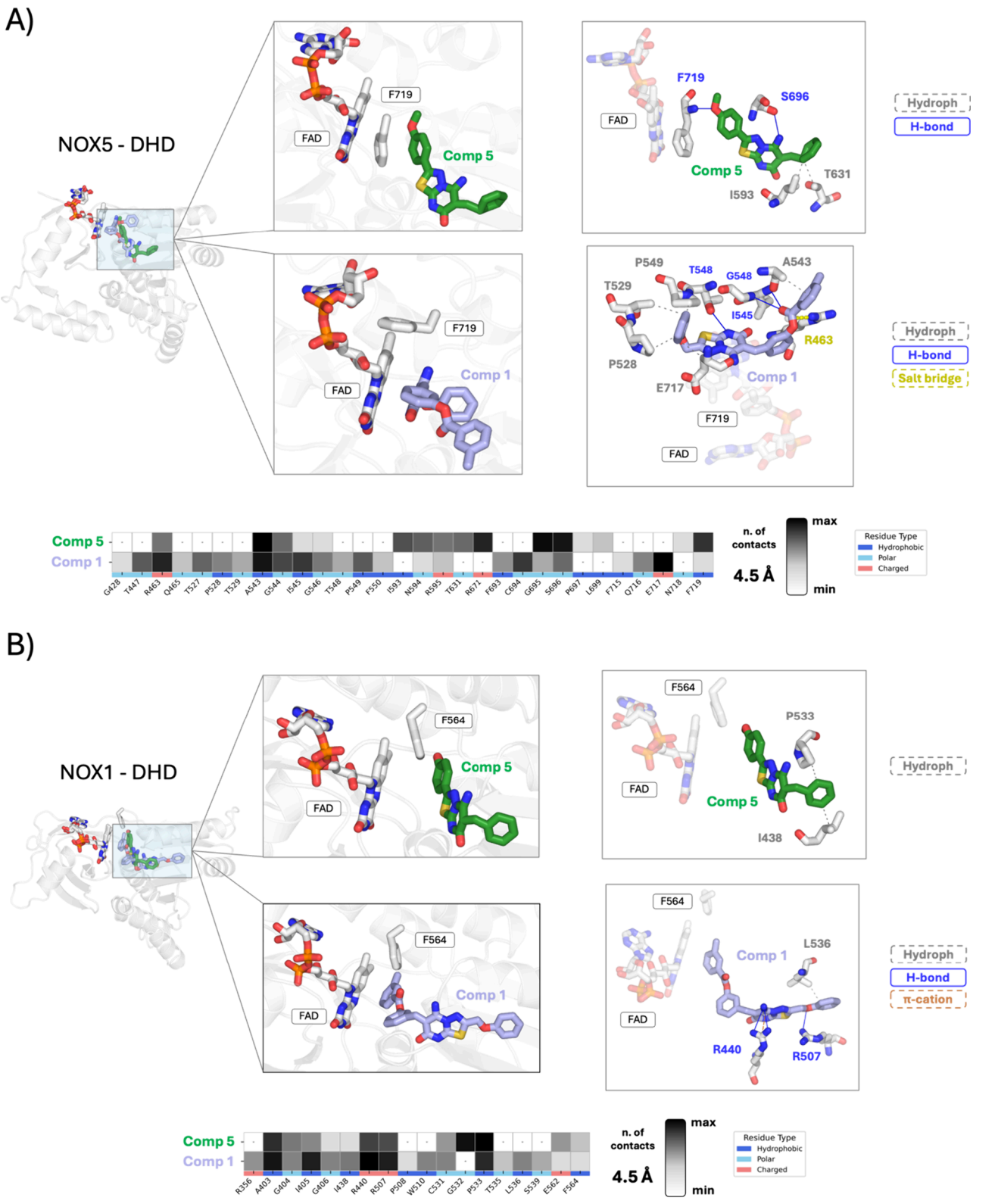

Figure 2. In A) and B), a cartoon representation of the Dehydrogenase domain (DHD) of NOX5 and NOX1 respectively, with zoomed perspectives on the binding mode of compound **5** (in green) and compound **1** (in light blue). The frames on the left represent overall positioning of both compounds relative to C-terminal residue and FAD, while the right frames indicate the computed noncovalent interactions. A comparative protein−ligand contact fingerprint of the compounds is represented below the frames, computed as the number of atoms of each residue that fall within a 4.5 Å cutoff. Missing contacts are represented with a dash.

cally significant protective effect in these cellular setups (data not shown).

To evaluate intrinsic neuroprotective and antioxidant properties beyond cellular models, compounds **1** and **5** were tested on rat brain subcellular fractions (Figures 4−6). In isolated

https://doi.org/10.1021/acsmedchemlett.6c00370
ACS Med. Chem. Lett. XXXX, XXX, XXX−XXX

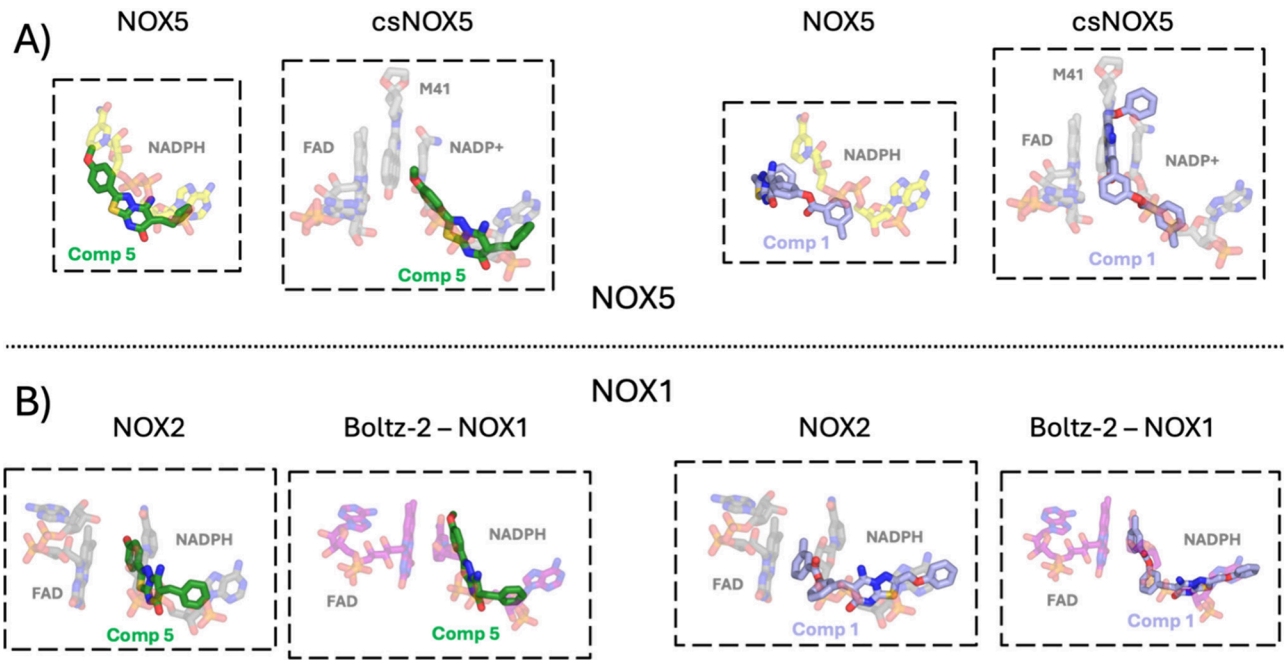

Figure 3. In A) superimpositions of the predicted NOX5-compound **5** and NOX5-compound **1** complexes against the cryo-EM NOX5 (PDB: 8U87) structure and homologous csNOX5-M41 complex (PDB: 8CB0). In B), superimpositions pertaining to the predicted NOX1 complexes, using the cryo-EM structure of NOX2 (PDB: 8WEJ) and a Boltz-2 generated model of the isoform.

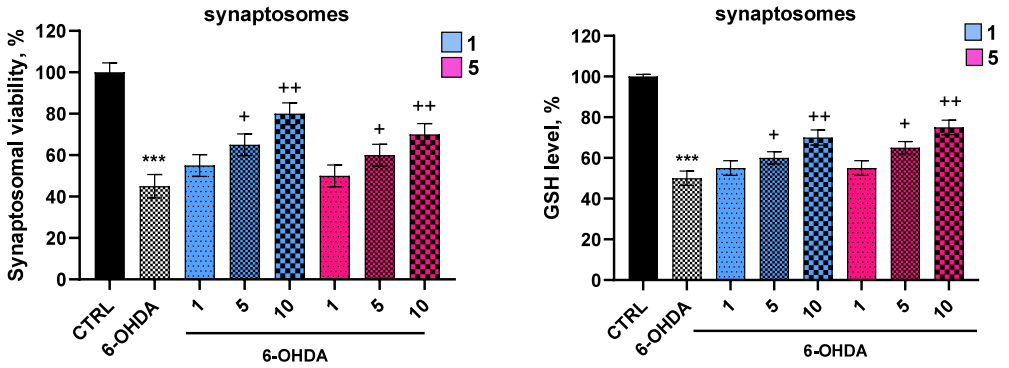

Figure 4. Neuroprotective effects of **1** and **5** (1−10 μM) against 6-OHDA-induced toxicity (150 μM) in rat brain synaptosomes. *P < 0.05; ***P < 0.001 vs control (nontreated synaptosomes). ^{+}P < 0.05; ^{+2}P < 0.01 vs control (6-OHDA).

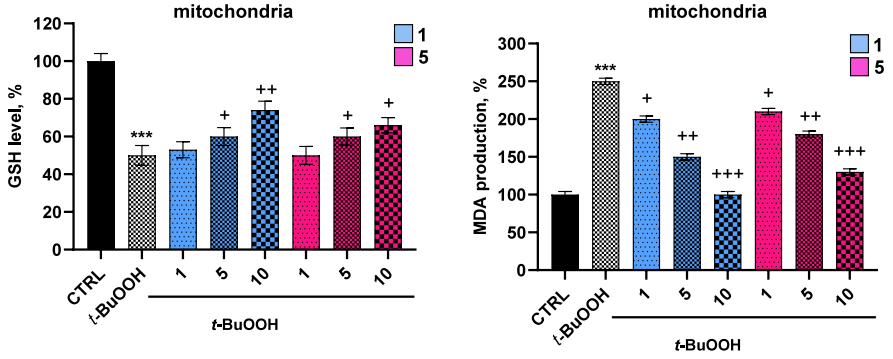

Figure 5. Effects of **1** and **5** (1−10 μM) on GSH and MDA levels in *t*-BuOOH-treated (75 μM) rat brain mitochondria. *P < 0.05; ***P < 0.001 vs control (nontreated mitochondria). ^{+}P < 0.05; ^{+2}P < 0.01 vs control (*t*-BuOOH).

synaptosomes, exposure to 6-hydroxydopamine (6-OHDA) (150 μM) significantly reduced viability and GSH levels by approximately 50%. Co-treatment with **1** or **5** (1−10 μM) concentration-dependently rescued both parameters, with **1** (10 μM) showing the highest efficacy by preserving 78% viability and 40% GSH (Figure 4).

In mitochondria, *tert*-butyl hydroperoxide (*t*-BuOOH) (75 μM) depleted GSH by 50% and increased MDA by 150%.

https://doi.org/10.1021/acsmedchemlett.6c00370
ACS Med. Chem. Lett. XXXX, XXX, XXX−XXX

Compounds **1** and **5** (1−10 μM) mitigated this oxidative damage; at 10 μM, **1** outperformed **5**, restoring GSH by 40% and suppressing MDA production by 60% (Figure 5).

Similarly, in microsomes subjected to Fe^{2+}/ascorbate-induced lipid peroxidation (which elevated MDA by 250%), both derivatives exhibited robust, concentration-dependent antioxidant profiles. At 10 μM, **1** and **5** decreased MDA formation by 66% and 57%, respectively, maintaining significant protective effects down to 1 μM (Figure 6).

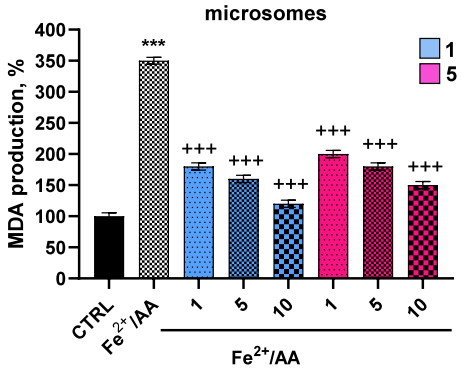

Figure 6. Antioxidant effects of **1** and **5** (1−10 μM) against Fe^{2+}/ascorbate-induced lipid peroxidation in rat brain microsomes. *P < 0.05; ***P < 0.001 vs control (nontreated microsomes). ^{+++}P < 0.001 vs control (Fe^{2+}/AA).

The compounds' influence on iron-mediated oxidative degradation of deoxyribose was subsequently assessed to check for secondary redox liabilities. Parental hit **1** exhibited a dose-dependent pro-oxidant effect, enhancing deoxyribose degradation from +3% at 10 μM up to 126.8% of the control at 100 μM (Figure 7). Conversely, the simplified analogue **5** demonstrated a negligible influence across the entire concentration range, showing a baseline 2% reduction at the highest dose (Figure 7). This indicates that molecular truncation favorably suppressed the iron-mediated pro-oxidant liability of the parent scaffold.

To dissect whether the biological outcomes stemmed from direct NOX enzyme inhibition or secondary radical-scavenging mechanisms, both derivatives were cross-screened in luminol-enhanced chemiluminescence (CL) assays using KO_2-generated superoxide anion radicals ($O_2^{\bullet-}$) and hypochlorite ions (ClO^-) (Figure 8).

Consistent with the deoxyribose data, **1** markedly enhanced the $O_2^{\bullet-}$ CL signal (+50% at 10 μM; 2-fold at 25 μM), signaling a structural propensity to drive oxidative processes (Figure 8A). Structural optimization successfully resolved this artifact; **5** exerted no stimulation at 10−25 μM and only a minor 11% increase at higher doses (Figure 8B), confirming improved mechanistic specificity and avoiding interference with physiological ROS signaling. In the ClO^- system, **1** remained inert, while **5** induced a modest, concentration-dependent signal reduction up to 20% at 25 μM (Figure 8C,D).

To completely rule out assay interference from direct, nonspecific radical quenching, horseradish peroxidase (HRP)-catalyzed oxidation of 2,2′-azino-bis(3-ethylbenzothiazoline-6-sulfonic acid (ABTS) by H_2O_2 was examined alongside a direct $ABTS^{\bullet+}$ scavenging control (Figure 9). Neither compound demonstrated intrinsic radical scavenging capacity against preformed $ABTS^{\bullet+}$ (Figure 9C,D; 99.78% for **1** and 101.28% for **5** at 25 μM). In the complete HRP/H_2O_2 enzymatic system, **1** triggered a minor, concentration-dependent decrease (5% at 25 μM), suggesting marginal interaction with H_2O_2 (Figure 9A), whereas **5** was totally inactive (Figure 9B). These chemical matrices collectively confirm that the structural optimization yielding **5** successfully stripped away the complex redox liabilities and pro-oxidant tendencies of the parental hit.

ANTIPROLIFERATIVE POTENTIAL IN CANCER CELL LINES

To explore the broader pathological relevance of NOX-dependent redox signaling in oncology, **1** and **5** were screened against a 10-dose panel of human cancer lines selected for distinct NOX expression profiles: Caco-2 (colorectal, NOX1-rich), SU-DHL-6 (lymphoma, NOX2-rich), RPMI-8226 (myeloma, NOX2-rich), HT-1080 (fibrosarcoma, NOX4-rich), and PSN1 (pancreatic, NOX5-rich) (Table 3).

Compound **1** demonstrated its most potent antiproliferative activity against the hematological lines SU-DHL-6 and RPMI-8226, yielding IC_{50} values of 13.8 and 18.0 μM, respectively

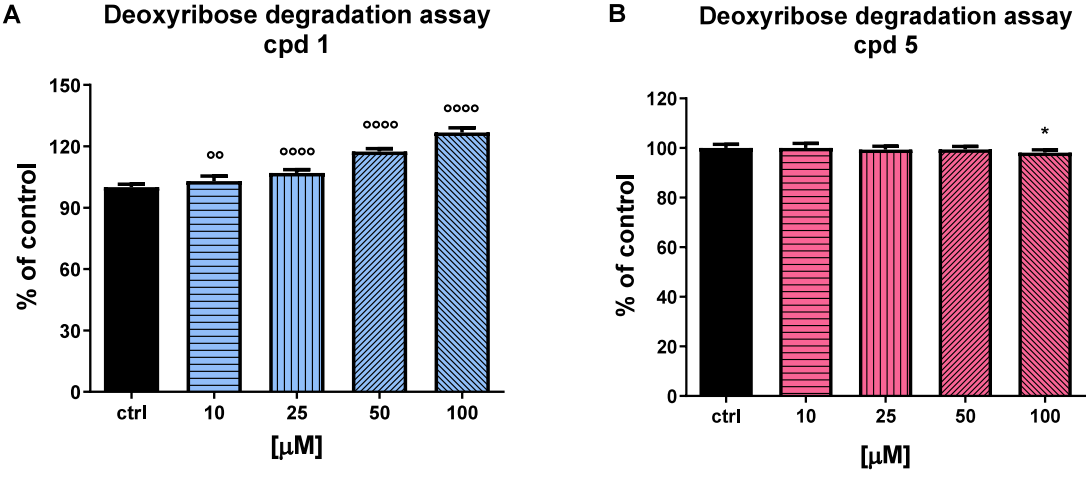

Figure 7. Concentration-dependent effect of the tested derivatives on iron-induced deoxyribose oxidative degradation. Data were analyzed using one-way ANOVA followed by Dunnett's post hoc test. The significance was set at $p \leq 0.05$. Significant decreases are indicated as asterisk (*) and significant increases by open circle (°) − */° $p \leq 0.05$, **/°° $p \leq 0.01$ and ****/°°°° $p \leq 0.0001$.

https://doi.org/10.1021/acsmedchemlett.6c00370
ACS Med. Chem. Lett. XXXX, XXX, XXX−XXX

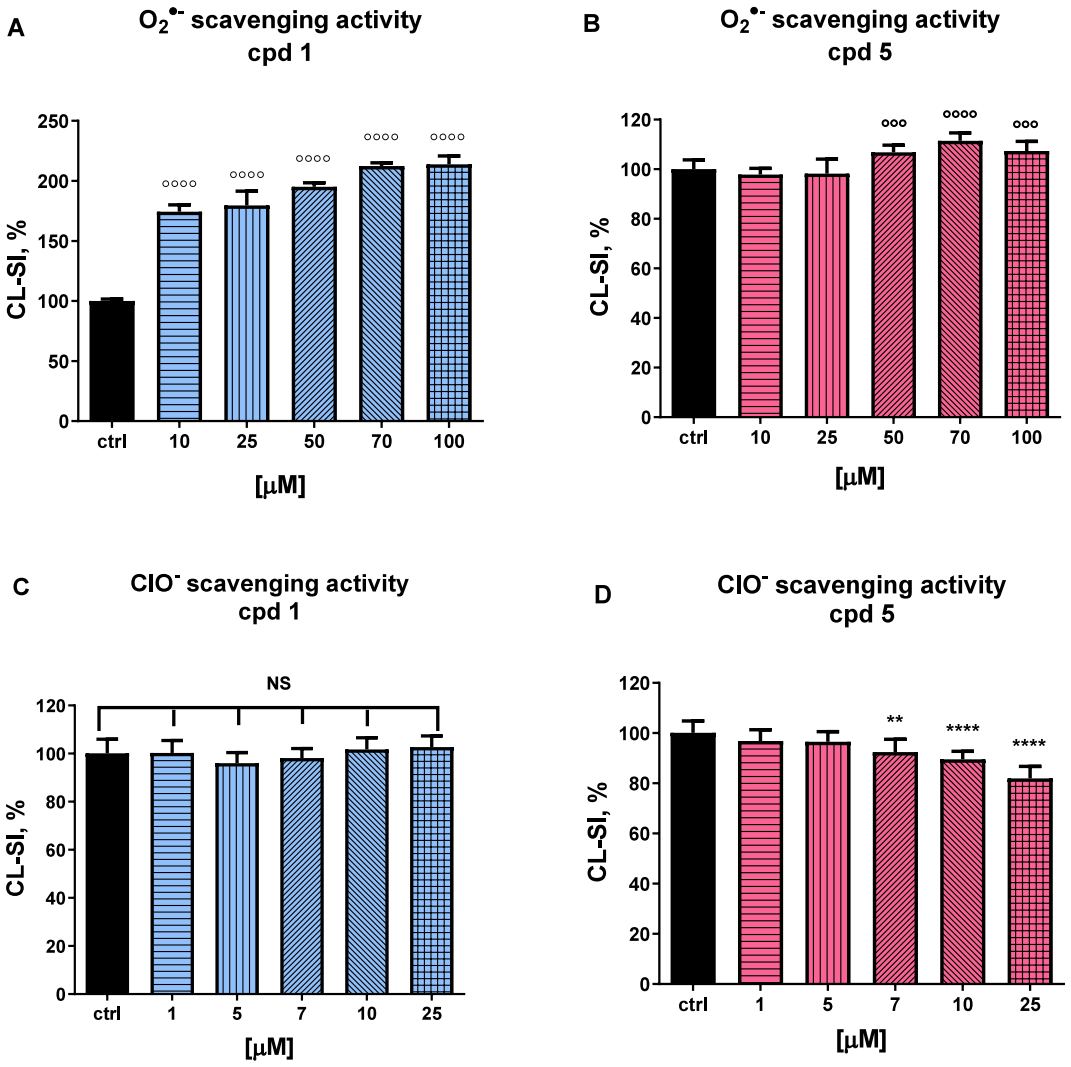

Figure 8. Concentration-dependent effect of the tested derivatives in chemiluminescent model systems: (A and B) System of KO_2-induced superoxide anion radical generation; (C and D) NaClO-induced hypochlorite ion generation. Results are expressed as mean ± SD of three independent replicates. Statistical significance was evaluated using one-way ANOVA followed by Dunnett's post hoc test, with significance level set at $p \leq 0.05$. Significantly lower or higher values were marked with * and ° respectively (NS − not significant; **/°° $p \leq 0.01$, ***/°°° $p \leq 0.001$ and ****/°°°° $p \leq 0.0001$).

(Table 3). This alignment strongly correlates with its preferential biochemical inhibition of NOX2 (IC_{50} = 16.7 μM, Table 2). Against solid tumor lines, **1** displayed 2- to 6-fold lower potencies. In stark contrast, the simplified analogue **5** exhibited a complete lack of antiproliferative activity across the entire panel, with IC_{50} values exceeding 60 μM in all cases (Table 3). This sharp drop in cellular efficacy reflects the poor aqueous solubility of **5**, which prevents the compound from reaching the high intracellular concentrations required to achieve effective maximal NOX inhibition, despite its promising cell-free biochemical IC_{50} parameters (Table 2). Antiproliferative curves relative to **1** and **5** in the tested cell lines are reported in Figure S4 in Supporting Information.

■ CONCLUSIONS

This study establishes clear, final structure−activity relationships for a novel series of [1,3,4]thiadiazolo[3,2-*a*]pyrimidine derivatives designed via a molecular striptease strategy. Extensive truncation of the heterocyclic core or removal of the peripheral 2-phenoxymethyl group (as in **6** and **7**) severely compromised NOX inhibition, underscoring the necessity of extended aromatic interactions within the dehydrogenase domain pocket. However, strategic optimization led to compound **5**, which bears a 4-methoxyphenyl group at the C2 position and a benzylidene motif at the C6 position. Compound **5** successfully retained the parental biochemical inhibitory profile against NOX2, NOX4, and DUOX1, while displaying an improved low-micromolar potency against NOX1 (IC_{50} = 9.0 μM) and NOX5 (IC_{50} = 11.3 μM), despite a low I_{max}.

The promising intrinsic neuroprotective profiles of **1** and **5** were confirmed in rat brain synaptosomes, mitochondria, and microsomes, where they effectively countered oxidative stress and lipid peroxidation at low micromolar concentrations. Crucially, in-depth evaluation across multiple ROS-generating chemical assays revealed that the structural simplification of **1** into **5** effectively eliminated the pro-oxidant liabilities and complex radical-scavenging artifacts inherent to the parent molecule, ensuring high mechanistic specificity. While **1** stands as a robust chemical probe with clear therapeutic potential against hematological malignancies, **5** represents a highly streamlined, clean chemotype. To overcome the physicochemical limitations of **5**, future optimization efforts will combine

https://doi.org/10.1021/acsmedchemlett.6c00370
ACS Med. Chem. Lett. XXXX, XXX, XXX−XXX

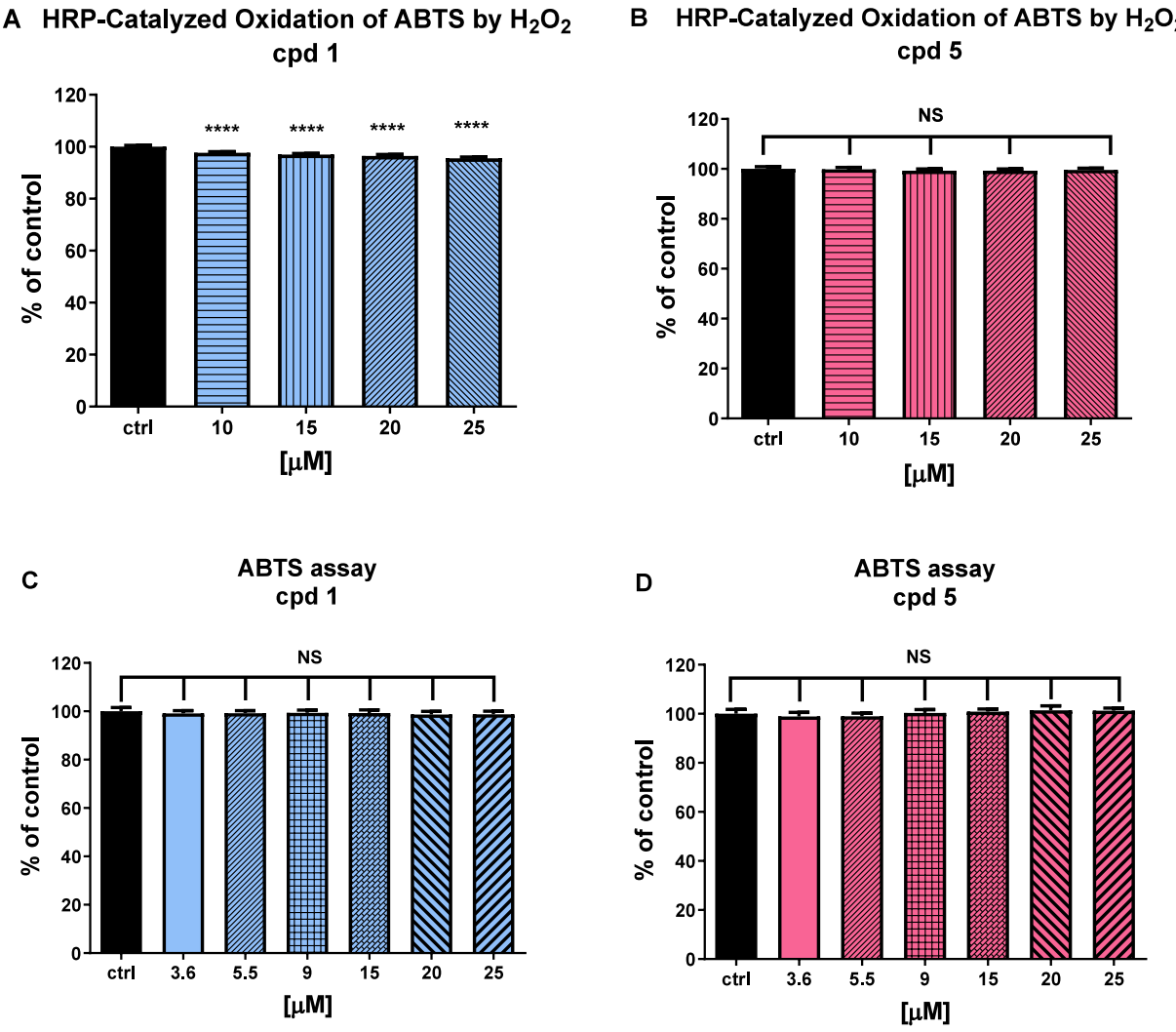

Figure 9. Concentration dependence of the HRP-Catalyzed Oxidation of ABTS by H_2O_2 in the presence of the tested NOX inhibitors (A and B) and control assessment of direct $ABTS^{\bullet+}$ radical scavenging as a potential interference (C and D). Data are reported as means ± SD from three independent measurements. Statistical significance was determined using one-way ANOVA (Dunnett's test). Significance level was set at $p \leq 0.05$. Significantly lower or higher values were marked with * and ° respectively (NS − not significant; and ****/°°°° $p \leq 0.0001$).

Table 3. Antiproliferative Effect of Compounds 1 and 5 in a Panel of Cancer Cells

	Antiproliferative activity, IC_{50}, μM				
compd	Caco-2 colorectal cancer	HT-1080 sarcoma	PSN1 pancreatic cancer	RPMI-8226 myeloma	SU-DHL-6 lymphoma
1	89.7	31.3	44.9	18.0	13.8
5	>200	71.7	185	81.5	60.1

prodrug strategies or hydrophilic formulations with rational structure-based modifications. Based on our docking analyses within the NADPH binding domain, key binding interactions are localized around the core scaffold, leaving vector positions on the outer rings oriented toward solvent-exposed regions. Consequently, the aqueous solubility of **5** can be systematically improved without disrupting crucial target engagements by (i) replacing the phenyl ring of the benzylidene moiety with basic nitrogen-containing heterocycles (such as pyridine or morpholine) or adding polar hydroxyl groups; (ii) modifying the methoxyphenyl ring with hydrophilic solubilizing handles, such as hydroxy group, short PEG-like chains or terminal aliphatic amines; or (iii) employing bioreversible prodrug strategies (e.g., phosphate or ester derivatives). Additionally, as **5** features an α/β-unsaturated system with theoretical Michael acceptor character, future optimization rounds will include thiol-reactivity assays (e.g., GSH binding) to confirm nonpromiscuous, reversible target interactions and rule out unspecific covalent labeling.

Once these solubility/reactivity bottlenecks are addressed, the scaffold of **5** can represent a highly promising, artifact-free architectural starting point for the development of potent, isoform-selective NOX inhibitors.

■ ASSOCIATED CONTENT

Supporting Information

The Supporting Information is available free of charge at https://pubs.acs.org/doi/10.1021/acsmedchemlett.6c00370.

Experimental Section: Synthetic procedures and analytical data of selected compounds, biochemical evaluation, computational methods, neuroprotective, antioxidant, and radical scavenging assays, anticancer assays. Inhib-

https://doi.org/10.1021/acsmedchemlett.6c00370
ACS Med. Chem. Lett. XXXX, XXX, XXX−XXX

ition curves for NOXs inhibition. Antiproliferative curves for tested cancer cell lines treated with 1 and 5 (PDF)

AUTHOR INFORMATION

Corresponding Author

Antonello Mai − *Department of Drug Chemistry and Technologies, Sapienza University of Rome, 00185 Rome, Italy;* orcid.org/0000-0001-9176-2382; Phone: +3906-4991-3392; Email: antonello.mai@uniroma1.it

Authors

Emanuele Fabbrizi − *Department of Drug Chemistry and Technologies, Sapienza University of Rome, 00185 Rome, Italy*

Andrea Mancini − *Department of Drug Chemistry and Technologies, Sapienza University of Rome, 00185 Rome, Italy*

Chiara Lambona − *Department of Drug Chemistry and Technologies, Sapienza University of Rome, 00185 Rome, Italy;* orcid.org/0000-0002-3415-4126

Salvatore Macrì − *Department of Drug Chemistry and Technologies, Sapienza University of Rome, 00185 Rome, Italy;* orcid.org/0009-0002-5853-9036

Marianna Nalli − *Department of Drug Chemistry and Technologies, Sapienza University of Rome, 00185 Rome, Italy*

Francesco Quilli − *Department of Molecular Medicine, Sapienza University of Rome, Laboratory Affiliated to Institut Pasteur - Cenci Bolognetti Foundation, 00161 Rome, Italy;* orcid.org/0009-0003-9635-1808

Federico Pandolfi − *Department of Molecular Medicine, Sapienza University of Rome, Laboratory Affiliated to Institut Pasteur - Cenci Bolognetti Foundation, 00161 Rome, Italy*

Domenico Raimondo − *Department of Molecular Medicine, Sapienza University of Rome, Laboratory Affiliated to Institut Pasteur - Cenci Bolognetti Foundation, 00161 Rome, Italy;* orcid.org/0000-0002-1780-7295

Sara Marchese − *Department of Biology and Biotechnology "Lazzaro Spallanzani", University of Pavia, 27100 Pavia, Italy;* orcid.org/0000-0002-9722-2616

Andrea Mattevi − *Department of Biology and Biotechnology "Lazzaro Spallanzani", University of Pavia, 27100 Pavia, Italy;* orcid.org/0000-0002-9523-7128

Jihyeon Lee − *Department of Life Science, Ewha Womans University, Seoul 120-750, South Korea; Celros Biotech, Rm 405, Science Building C, Seoul 120-750, South Korea*

Minhye Choi − *Department of Life Science, Ewha Womans University, Seoul 120-750, South Korea; Celros Biotech, Rm 405, Science Building C, Seoul 120-750, South Korea*

Yun Soo Bae − *Department of Life Science, Ewha Womans University, Seoul 120-750, South Korea; Celros Biotech, Rm 405, Science Building C, Seoul 120-750, South Korea*

Nadya Hristova-Avakumova − *Department of Medical Physics and Biophysics, Faculty of Medicine, Medical University of Sofia, 1431 Sofia, Bulgaria*

Magdalena Kondeva-Burdina − *Laboratory of Drug Metabolism and Drug Toxicity, Department of Pharmacology, Pharmacotherapy and Toxicology, Faculty of Pharmacy, Medical University-Sofia, 1000 Sofia, Bulgaria*

Denitsa Stefanova − *Laboratory of Drug Metabolism and Drug Toxicity, Department of Pharmacology, Pharmacotherapy and Toxicology, Faculty of Pharmacy, Medical University-Sofia, 1000 Sofia, Bulgaria*

Neda Anastassova − *Institute of Organic Chemistry with Centre of Phytochemistry, Bulgarian Academy of Sciences, 1113 Sofia, Bulgaria;* orcid.org/0000-0002-2776-0021

Sergio Valente − *Department of Drug Chemistry and Technologies, Sapienza University of Rome, 00185 Rome, Italy;* orcid.org/0000-0002-2241-607X

Dante Rotili − *Department of Science, Roma Tre University, 00146 Rome, Italy; Biostructures and Biosystems National Institute (INBB), 00165 Rome, Italy;* orcid.org/0000-0002-8428-8763

Complete contact information is available at: https://pubs.acs.org/10.1021/acsmedchemlett.6c00370

Author Contributions

¶E.F. and A. M. equally contributed to this work.

Notes

The authors declare no competing financial interest.

ACKNOWLEDGMENTS

Research on NOX proteins was supported by the Associazione Italiana per la Ricerca sul Cancro (AIRC; IG31139 to A. Mai), AIRC Fellowship on NOXs (28098 to S. Marchese), MUR (PRIN PNRR 2022 P2022FESRR_002 to A. Mai and A. Mattevi). This research was supported by NRF grants (RS-2024-00398295 to Y.S.B.) funded by the Ministry of Science and ICT, Republic of Korea.

ABBREVIATIONS

ABTS, 2,2′-azino-bis(3-ethylbenzothiazoline-6-sulfonic acid; ANOVA, One-way analysis of variance; apo, apoprotein; *t*-BuOOH, *tert*-butyl hydroperoxide; CL, chemiluminescence; Cryo-EM, cryo-electron microscopy; *cs*, *Cylindrospermum stagnale*; DHD, dehydrogenase domain; DUOX, dual oxidase; Fe^{2+}/AA, Fe^{2+}/ascorbate; GSH, reduced glutathione; HRP, horseradish peroxidase; I_{max}, maximum inhibition; KO_2, potassium superoxide; MPP^+, 1-methyl-4-phenylpyridinium; MTT, 3-[4,5-dimethylthiazol-2-yl]-2,5-diphenyltetrazolium bromide; NaClO, sodium hypochlorite; NOX, NADPH oxidase; $O_2^{\bullet-}$, superoxide radicals; 6-OHDA, 6-hydroxydopamine

REFERENCES

(1) Mattson, M. P. Apoptosis in neurodegenerative disorders. *Nat. Rev. Mol. Cell Biol.* **2000**, *1* (2), 120−129 From NLM Medline.

(2) Heneka, M. T.; Carson, M. J.; El Khoury, J.; Landreth, G. E.; Brosseron, F.; Feinstein, D. L.; Jacobs, A. H.; Wyss-Coray, T.; Vitorica, J.; Ransohoff, R. M.; et al. Neuroinflammation in Alzheimer's disease. *Lancet Neurol* **2015**, *14* (4), 388−405 From NLM Medline.

(3) Lin, M. T.; Beal, M. F. Mitochondrial dysfunction and oxidative stress in neurodegenerative diseases. *Nature* **2006**, *443* (7113), 787−795 From NLM Medline.

(4) Andersen, J. K. Oxidative stress in neurodegeneration: cause or consequence? *Nat. Med.* **2004**, *10* (S7), S18−25 From NLM Medline.

(5) Bedard, K.; Krause, K. H. The NOX family of ROS-generating NADPH oxidases: physiology and pathophysiology. *Physiol Rev.* **2007**, *87* (1), 245−313 From NLM Medline.

(6) Sorce, S.; Krause, K. H. NOX enzymes in the central nervous system: from signaling to disease. *Antioxid Redox Signal* **2009**, *11* (10), 2481−2504 From NLM Medline.

(7) Block, M. L.; Zecca, L.; Hong, J. S. Microglia-mediated neurotoxicity: uncovering the molecular mechanisms. *Nat. Rev. Neurosci* **2007**, *8* (1), 57−69 From NLM Medline.

https://doi.org/10.1021/acsmedchemlett.6c00370
ACS Med. Chem. Lett. XXXX, XXX, XXX−XXX

(8) Wilkinson, B. L.; Landreth, G. E. The microglial NADPH oxidase complex as a source of oxidative stress in Alzheimer's disease. *J. Neuroinflammation* **2006**, *3*, 30 From NLM PubMed-not-MEDLINE.
(9) Lambeth, J. D. NOX enzymes and the biology of reactive oxygen. *Nat. Rev. Immunol* **2004**, *4* (3), 181−189 From NLM Medline.
(10) Wu, D. C.; Teismann, P.; Tieu, K.; Vila, M.; Jackson-Lewis, V.; Ischiropoulos, H.; Przedborski, S. NADPH oxidase mediates oxidative stress in the 1-methyl-4-phenyl-1,2,3,6-tetrahydropyridine model of Parkinson's disease. *Proc. Natl. Acad. Sci. U. S. A.* **2003**, *100* (10), 6145−6150 From NLM Medline.
(11) Gao, H. M.; Hong, J. S. Why neurodegenerative diseases are progressive: uncontrolled inflammation drives disease progression. *Trends Immunol* **2008**, *29* (8), 357−365 From NLM Medline.
(12) Hernandes, M. S.; Britto, L. R. NADPH oxidase and neurodegeneration. *Curr. Neuropharmacol* **2012**, *10* (4), 321−327 From NLM PubMed-not-MEDLINE.
(13) Drummond, G. R.; Selemidis, S.; Griendling, K. K.; Sobey, C. G. Combating oxidative stress in vascular disease: NADPH oxidases as therapeutic targets. *Nat. Rev. Drug Discov* **2011**, *10* (6), 453−471 From NLM Medline.
(14) Konate, M. M.; Antony, S.; Doroshow, J. H. Inhibiting the Activity of NADPH Oxidase in Cancer. *Antioxid Redox Signal* **2020**, *33* (6), 435−454 From NLM Medline.
(15) Marques, J.; Fernandez-Irigoyen, J.; Ainzua, E.; Martinez-Azcona, M.; Cortes, A.; Roncal, C.; Orbe, J.; Santamaria, E.; Zalba, G. NADPH Oxidase 5 (NOX5) Overexpression Promotes Endothelial Dysfunction via Cell Apoptosis, Migration, and Metabolic Alterations in Human Brain Microvascular Endothelial Cells (hCMEC/D3). *Antioxidants (Basel)* **2022**, *11* (11), 2147 From NLM PubMed-not-MEDLINE.
(16) Damiano, S.; Fusco, R.; Morano, A.; De Mizio, M.; Paterno, R.; De Rosa, A.; Spinelli, R.; Amente, S.; Frunzio, R.; Mondola, P.; et al. Reactive oxygen species regulate the levels of dual oxidase (Duox1−2) in human neuroblastoma cells. *PLoS One* **2012**, *7* (4), No. e34405, From NLM Medline.
(17) Ameziane-El-Hassani, R.; Talbot, M.; de Souza Dos Santos, M. C.; Al Ghuzlan, A.; Hartl, D.; Bidart, J. M.; De Deken, X.; Miot, F.; Diallo, I.; de Vathaire, F.; et al. NADPH oxidase DUOX1 promotes long-term persistence of oxidative stress after an exposure to irradiation. *Proc. Natl. Acad. Sci. U. S. A.* **2015**, *112* (16), 5051−5056 From NLM Medline.
(18) Chen, J.; Wang, Y.; Zhang, W.; Zhao, D.; Zhang, L.; Fan, J.; Li, J.; Zhan, Q. Membranous NOX5-derived ROS oxidizes and activates local Src to promote malignancy of tumor cells. *Signal Transduct Target Ther* **2020**, *5* (1), 139 From NLM Medline.
(19) Gorgulla, C.; Boeszoermenyi, A.; Wang, Z. F.; Fischer, P. D.; Coote, P. W.; Padmanabha Das, K. M.; Malets, Y. S.; Radchenko, D. S.; Moroz, Y. S.; Scott, D. A.; et al. An open-source drug discovery platform enables ultra-large virtual screens. *Nature* **2020**, *580* (7805), 663−668 From NLM Medline.
(20) Reis, J.; Gorgulla, C.; Massari, M.; Marchese, S.; Valente, S.; Noce, B.; Basile, L.; Torner, R.; Cox, H., 3rd; Viennet, T.; et al. Targeting ROS production through inhibition of NADPH oxidases. *Nat. Chem. Biol.* **2023**, *19* (12), 1540−1550 From NLM Medline.
(21) Hann, M. M.; Keseru, G. M. Finding the sweet spot: the role of nature and nurture in medicinal chemistry. *Nat. Rev. Drug Discov* **2012**, *11* (5), 355−365 From NLM Medline.
(22) Lovering, F.; Bikker, J.; Humblet, C. Escape from flatland: increasing saturation as an approach to improving clinical success. *J. Med. Chem.* **2009**, *52* (21), 6752−6756 From NLM Medline.
(23) Joo, J. H.; Huh, J. E.; Lee, J. H.; Park, D. R.; Lee, Y.; Lee, S. G.; Choi, S.; Lee, H. J.; Song, S. W.; Jeong, Y.; et al. A novel pyrazole derivative protects from ovariectomy-induced osteoporosis through the inhibition of NADPH oxidase. *Sci. Rep* **2016**, *6*, 22389 From NLM Medline.
(24) Magnani, F.; Nenci, S.; Millana Fananas, E.; Ceccon, M.; Romero, E.; Fraaije, M. W.; Mattevi, A. Crystal structures and atomic model of NADPH oxidase. *Proc. Natl. Acad. Sci. U. S. A.* **2017**, *114* (26), 6764−6769 From NLM Medline.
(25) Ogboo, B. C.; Grabovyy, U. V.; Maini, A.; Scouten, S.; van der Vliet, A.; Mattevi, A.; Heppner, D. E. Architecture of the NADPH oxidase family of enzymes. *Redox Biol.* **2022**, *52*, 102298 From NLM Medline.
(26) Cui, C.; Jiang, M.; Jain, N.; Das, S.; Lo, Y. H.; Kermani, A. A.; Pipatpolkai, T.; Sun, J. Structural basis of human NOX5 activation. *Nat. Commun.* **2024**, *15* (1), 3994 From NLM Medline.
(27) Zhen, L.; Yu, L.; Dinauer, M. C. Probing the role of the carboxyl terminus of the gp91phox subunit of neutrophil flavocytochrome b558 using site-directed mutagenesis. *J. Biol. Chem.* **1998**, *273* (11), 6575−6581 From NLM Medline.
(28) Liu, X.; Shi, Y.; Liu, R.; Song, K.; Chen, L. Structure of human phagocyte NADPH oxidase in the activated state. *Nature* **2024**, *627* (8002), 189−195 From NLM Medline.
(29) Arbo, M. D.; Silva, R.; Barbosa, D. J.; Dias da Silva, D.; Silva, S. P.; Teixeira, J. P.; Bastos, M. L.; Carmo, H. In vitro neurotoxicity evaluation of piperazine designer drugs in differentiated human neuroblastoma SH-SY5Y cells. *J. Appl. Toxicol* **2016**, *36* (1), 121−130 From NLM Medline.
(30) Pandey, M.; Karmakar, V.; Majie, A.; Dwivedi, M.; Md, S.; Gorain, B. The SH-SY5Y cell line: a valuable tool for Parkinson's disease drug discovery. *Expert Opin Drug Discov* **2024**, *19* (3), 303−316 From NLM Medline.

https://doi.org/10.1021/acsmedchemlett.6c00370
ACS Med. Chem. Lett. XXXX, XXX, XXX−XXX